Electronic Supplementary Material (ESI) for Soft Matter

Scalable Synthesis of Self-Assembling Nanoparticle Clusters Based on Controlled Steric Interactions

Kjersta Larson-Smith and Danilo C. Pozzo*

Supplementary Information

PEG Grafting Density Determination

The dose concentration range of PEG chains over which systematic changes in clustering occur is much larger than what is typically needed to saturate a gold surface.[1] The actual amount of PEG bound to the gold surface is expected to be much lower, so the activity of the thiol and kinetics of binding are impacting the necessary dose concentrations. To determine the activity of the PEG-thiol, dialyzed samples are studied using Thermo Gravimetric Analysis (TGA). The samples are pressure filtered through a dialysis membrane with 50kDa NMWL pores for a total of twenty times to remove any un-reacted PEG-thiol remaining in solution. Samples are then lyophilized to remove the water. The change in sample weight as a function of temperature is examined using a TA Instruments Q50 TGA with a heating rate of 20°Cmin^{-1} from room temperature to 600°C in nitrogen. Samples containing total dose concentrations of 2.9-14.7 PEG chains/nm^2 Au are measured with TGA and the results are shown in Figure S1. The drop at 300-360°C for the samples indicates a loss of the PEG-thiol while the remaining weight in the sample is the gold particles. The actual PEG concentration is determined from these plots for each sample and reported in Table S1. The average activity of the PEG-thiol is 12.4 ± 1.2% and all dose PEG concentrations reported in this work are scaled according to this value. The clustering of the particles is identical before and after removing un-reacted PEG-thiol as shown with Small-Angle X-ray Scattering in Figure S2.

Table S1. Determination of PEG-thiol activity by TGA for filtered and lyophilized samples.

Dose PEG Concentration (chains/nm^2 Au)	Measured wt% Au	Measured wt% PEG	Actual PEG Concentration (chains/nm2 Au)	% Active PEG
14.7	56.68	43.32	1.64	11.19
7.8	66.44	33.56	1.09	13.94
6.7	73.82	26.18	0.76	11.39
4.8	79.98	20.02	0.54	11.22
2.9	85.26	14.74	0.37	12.83

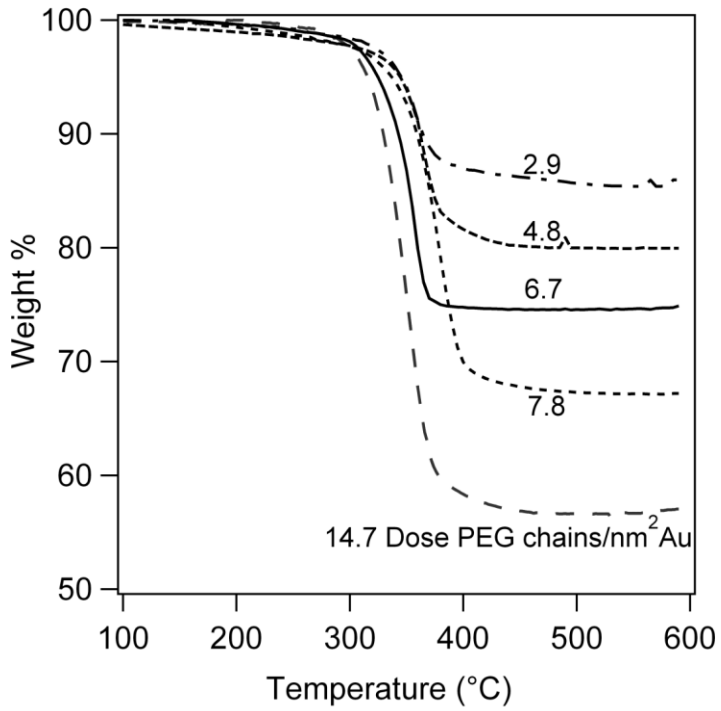

Figure S1. TGA of PEG functionalized gold samples that are filtered twenty times and lyophilized.

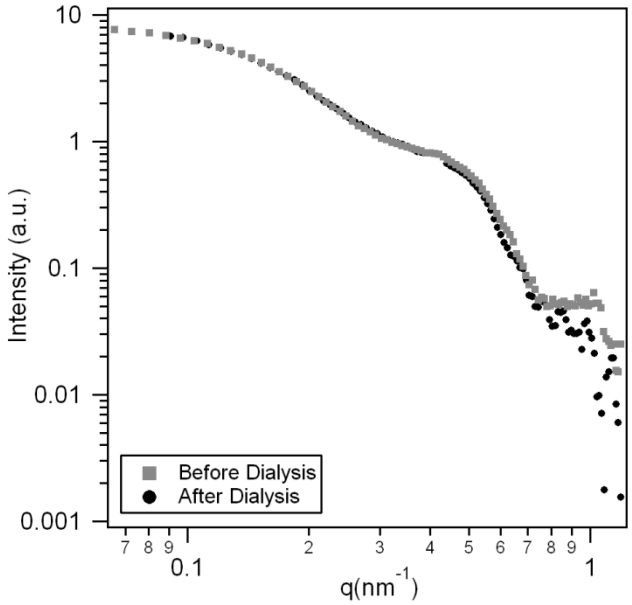

Figure S2. SAXS experimental curves for octane functionalized 0.8 PEG chains/nm^2 Au clusters before and after dialysis.

Gold Raft Formation

In addition to clustering, the amphiphilic particles that we produce in this work also adsorb at the air-water interface. The adsorption is very evident from the formation of rafts that form a gold sheen at the interface. The rafts form for all PEG loadings, even at the PEG saturation point when only singlets form in dispersion. One possible explanation for this phenomenon is that the particles are amphiphilic.

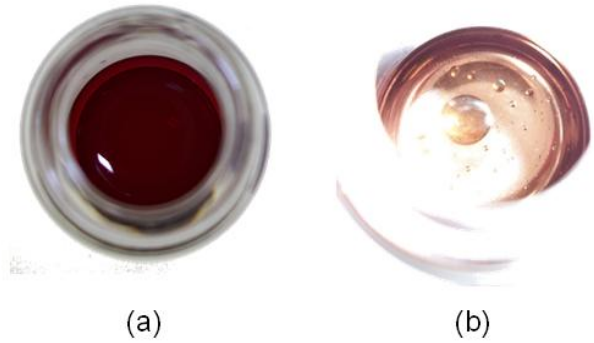

Figure S3. Photographs of the air-water interface for 1.0 PEG chain/nm2Au (a) before and (b) after octane-thiol addition illustrates the formation of rafts.

Small-Angle X-ray Scattering Models

Simple geometric models are used to quantitatively understand Small Angle X-ray Scattering (SAXS) profiles. The models are derived from the fundamental Debye Equation and Rayleigh's equation for spherical particles.[2, 3] Equation 1 is a simplified Debye Equation for particles consisting of spherical subunits.[4] F(q) is the scattering contributions for a sphere given by Equation 2, where R is the particle radius and q is the scattering vector. In these equations, r_{ij} is the separation distance between the centers of particles i and j. Models are developed for nine possible cluster geometries: doublet (Equation 3), triplet (Equation 4), tetrahedral (Equation 5), trigonal dipyramidal (Equation 6), octahedral (Equation 7), pentagonal dipyramidal (Equation 8), snub disphenoid (Equation 9), triaugmented triangular prism (Equation 10) and gyroelongated square dipyramid (Equation 11). For each configuration, x is the nearest neighbor separation distance. As an example, a schematic of the particle separation distance determination for each model is shown in Figures S4-S10.

$$I(q) = \sum_{i=1}^{N} F_i(q)^2 + 2\sum_{i=1}^{N-1}\sum_{j=i+1}^{N} F_i(q)F_j(q)\frac{sinqr_{ij}}{qr_{ij}} \quad (1)$$

$$F(q) = \frac{3[\sin(qR) - qR\cos(qR)]}{(qR)^3} \quad (2)$$

$$I(q) = F(q)^2\left[2 + 2\frac{\sin(qx)}{qx}\right] \quad (3)$$

$$I(q) = F(q)^2\left[3 + 6\frac{\sin(qx)}{qx}\right] \quad (4)$$

$$I(q) = F(q)^2\left[4 + 12\frac{\sin(qx)}{qx}\right] \quad (5)$$

$$I(q) = F(q)^2\left[5 + 18\frac{\sin(qx)}{qx} + 2\frac{\sin(\sqrt{8/3}\,qx)}{\sqrt{8/3}\,qx}\right] \quad (6)$$

$$I(q) = F(q)^2\left[6 + 24\frac{\sin(qx)}{qx} + 6\frac{\sin(\sqrt{2}qx)}{\sqrt{2}qx} + \right] \quad (7)$$

$$I(q) = F(q)^2\left[7 + 30\frac{\sin(qx)}{qx} + 10\frac{\sin(1.618qx)}{1.618qx} + 2\frac{\sin(1.052qx)}{1.052qx}\right] \quad (8)$$

$$I(q) = F(q)^2\left[8 + 36\frac{\sin(qx)}{qx} + 18\frac{\sin(1.513qx)}{1.513qx} + 2\frac{\sin(1.289qx)}{1.289qx}\right] \quad (9)$$

$$I(q) = F(q)^2\left[9 + 42\frac{\sin(qx)}{qx} + 12\frac{\sin(\sqrt{2}qx)}{\sqrt{2}qx} + 12\frac{\sin(1.651qx)}{1.651qx} + 6\frac{\sin(1.725qx)}{1.725qx}\right] \quad (10)$$

$$I(q) = F(q)^2\left[10 + 48\frac{\sin(qx)}{qx} + 8\frac{\sin(\sqrt{2}qx)}{\sqrt{2}qx} + 16\frac{\sin(1.554qx)}{1.554qx} + 16\frac{\sin(1.702qx)}{1.702qx} + 2\frac{\sin(2.255qx)}{2.255qx}\right] \quad (11)$$

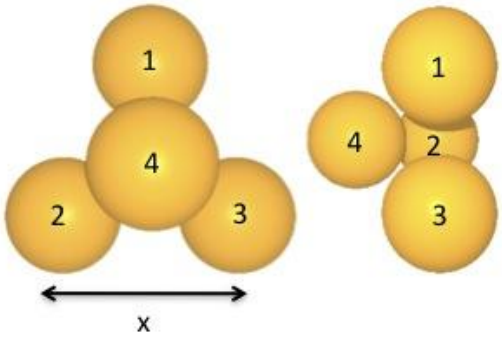

$$r_{12} = r_{23} = r_{13} = r_{14} = r_{24} = r_{34} = x$$

Figure S4. Schematic of tetrahedral cluster and corresponding particle separation distances.

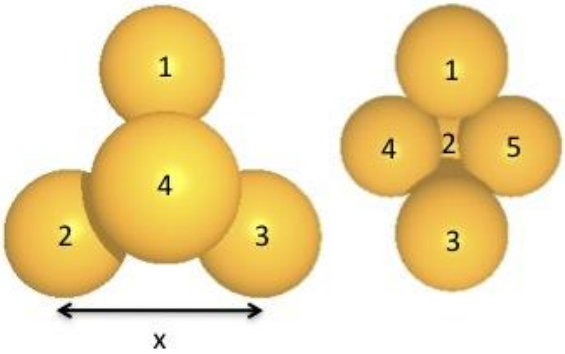

$$r_{12} = r_{23} = r_{13} = r_{14} = r_{24} = r_{34} = r_{15} = r_{25} = r_{35} = x$$

$$r_{45} = \sqrt{8/3}\,x$$

Figure S5. Schematic of trigonal dipyramid cluster and corresponding particle separation distances.

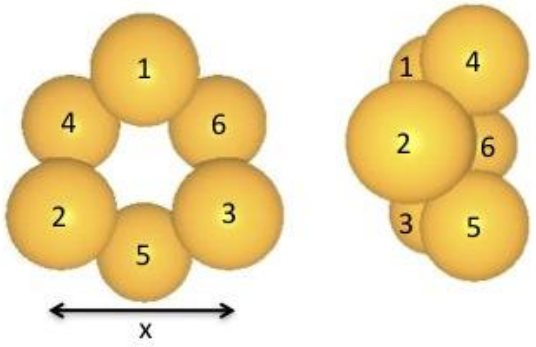

$$r_{12} = r_{23} = r_{13} = r_{45} = r_{56} = r_{46} =$$
$$r_{14} = r_{16} = r_{24} = r_{25} = r_{35} = r_{36} = x$$

$$r_{15} = r_{26} = r_{34} = \sqrt{2}x$$

Figure S6. Schematic of octahedral cluster and corresponding particle separation distances.

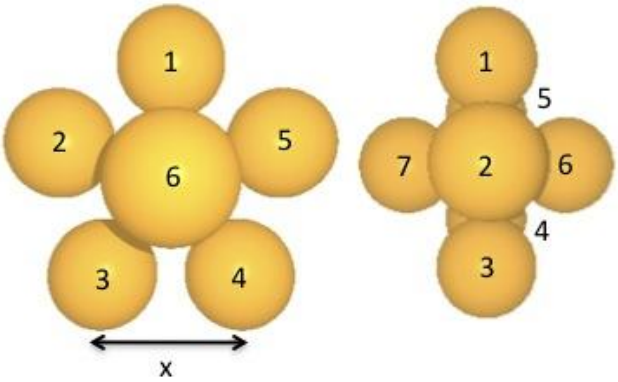

$$r_{12} = r_{23} = r_{34} = r_{45} = r_{15} =$$
$$r_{16} = r_{26} = r_{36} = r_{46} = r_{56} =$$
$$r_{17} = r_{27} = r_{37} = r_{47} = r_{57} = x$$

$$r_{13} = r_{14} = r_{24} = r_{25} = r_{35} = 1.618x$$

$$r_{67} = 1.0515x$$

Figure S7. Schematic of pentagonal dipyramid cluster and corresponding particle separation distances.

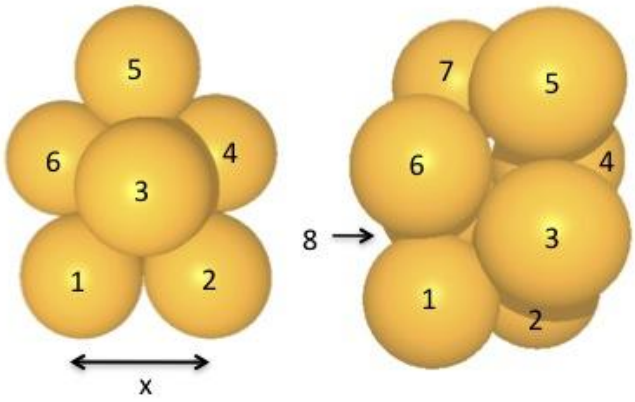

$$r_{12} = r_{24} = r_{45} = r_{56} = r_{16} = r_{47} = r_{67} =$$
$$r_{13} = r_{23} = r_{34} = r_{35} = r_{36} = r_{18} = r_{28} =$$
$$r_{48} = r_{68} = r_{78} = r_{57} = x$$

$$r_{14} = r_{15} = r_{17} = r_{26} = r_{25} =$$
$$r_{27} = r_{37} = r_{46} = r_{58} = 1.513x$$

$$r_{58} = 1.289x$$

Figure S8. Schematic of snub disphenoid cluster and corresponding particle separation distances.

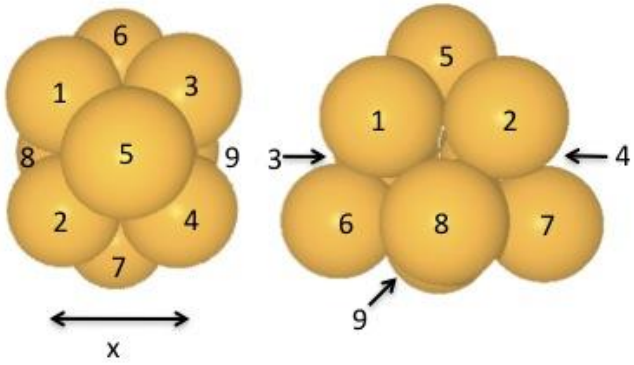

$$r_{12} = r_{13} = r_{15} = r_{16} = r_{18} = r_{24} = r_{25} =$$
$$r_{27} = r_{28} = r_{34} = r_{35} = r_{36} = r_{39} = r_{45} =$$
$$r_{47} = r_{49} = r_{67} = r_{68} = r_{69} = r_{78} = r_{79} = x$$
$$r_{14} = r_{17} = r_{23} = r_{26} = r_{37} = r_{46} = 1.414x$$
$$r_{19} = r_{29} = r_{38} = r_{48} = r_{56} = r_{57} = 1.651x$$
$$r_{58} = r_{59} = r_{89} = 1.725x$$

Figure S9. Schematic of triaugmented triangular prism cluster and corresponding particle separation distances.

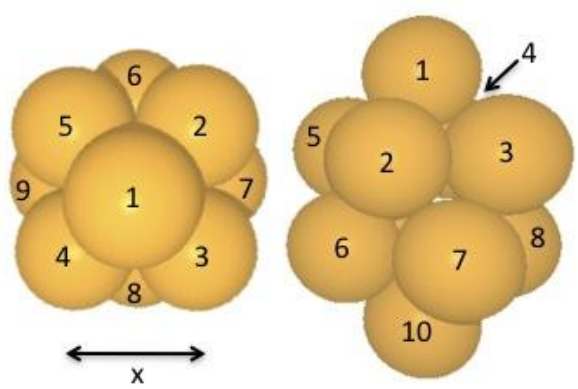

$$r_{12} = r_{13} = r_{14} = r_{15} = r_{23} = r_{25} = r_{26} = r_{27} =$$
$$r_{34} = r_{36} = r_{39} = r_{45} = r_{48} = r_{49} = r_{57} = r_{58} =$$
$$r_{67} = r_{69} = r_{610} = r_{78} = r_{710} = r_{89} = r_{810} = r_{910} = x$$
$$r_{24} = r_{35} = r_{68} = r_{79} = 1.414x$$
$$r_{28} = r_{29} = r_{37} = r_{38} = r_{46} = r_{47} = r_{56} = r_{59} = 1.554x$$
$$r_{16} = r_{17} = r_{18} = r_{19} = r_{210} = r_{310} = r_{410} = r_{510} = 1.702x$$
$$r_{110} = 2.255x$$

Figure S10. Schematic of gyroelongated square dipyramid cluster and corresponding particle separation distances.

Predicted scattering curves are created by weighting the scattering models by the histograms that are generated from Transmission Electron Microscopy (TEM) data. As shown in Figure 8, there is remarkable agreement between the predicted and measured curves. The limitation of SAXS is that it is always affected by polydispersity. Therefore, SAXS alone (i.e. without TEM) is not enough to fully characterize polydisperse clusters in dispersion. Figure S11 shows the sensitivity of the scattering data to the weighting of the distribution. Figure S11a shows the calculated SAXS predictions for Gaussian distributions that are centered on various mean cluster sizes with a variance of 1. This calculation shows that the SAXS data is quite sensitive to the average number of particles/cluster. However, Figure S11b shows that SAXS is less sensitive to the broadness of the distribution. The primary differences in scattering with similar mean but different variance are observed in the dip at $q=0.35nm^{-1}$ which will also be affected by instrumental smearing. In all of these calculations, the prediction obtained from the experimental TEM histograms shows the best agreement with the data.

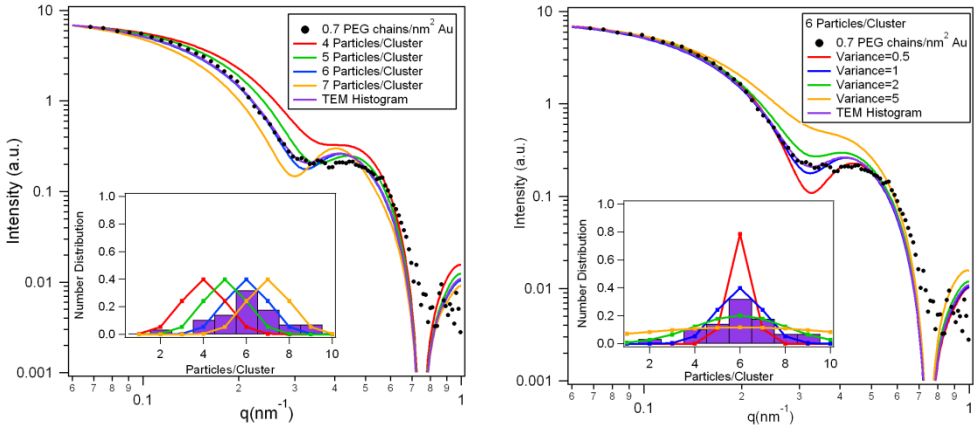

a b

Figure S11. Modeled SAXS curves based on arbitrarily created Gaussian distributions to test the model sensitivity to (a) number of particles/cluster and (b) variance.

Transmission Electron Microscopy

TEM of dried dispersions is used to characterize the structures of the nanoparticle clusters. Unfortunately, the drying process leads to changes in the cluster structures because of the collapse of the polymer layer. Still, we are able to determine the number of particles in each cluster. For this study, tens of images are taken for 6 samples and a histogram is generated to quantify the number of particles in each cluster. It is clear that there is a distribution of cluster sizes for each sample, but we still observe that the average number of particles per cluster scales inversely with PEG concentration. The histograms and a sampling of TEM micrographs are shown in Figure S12.

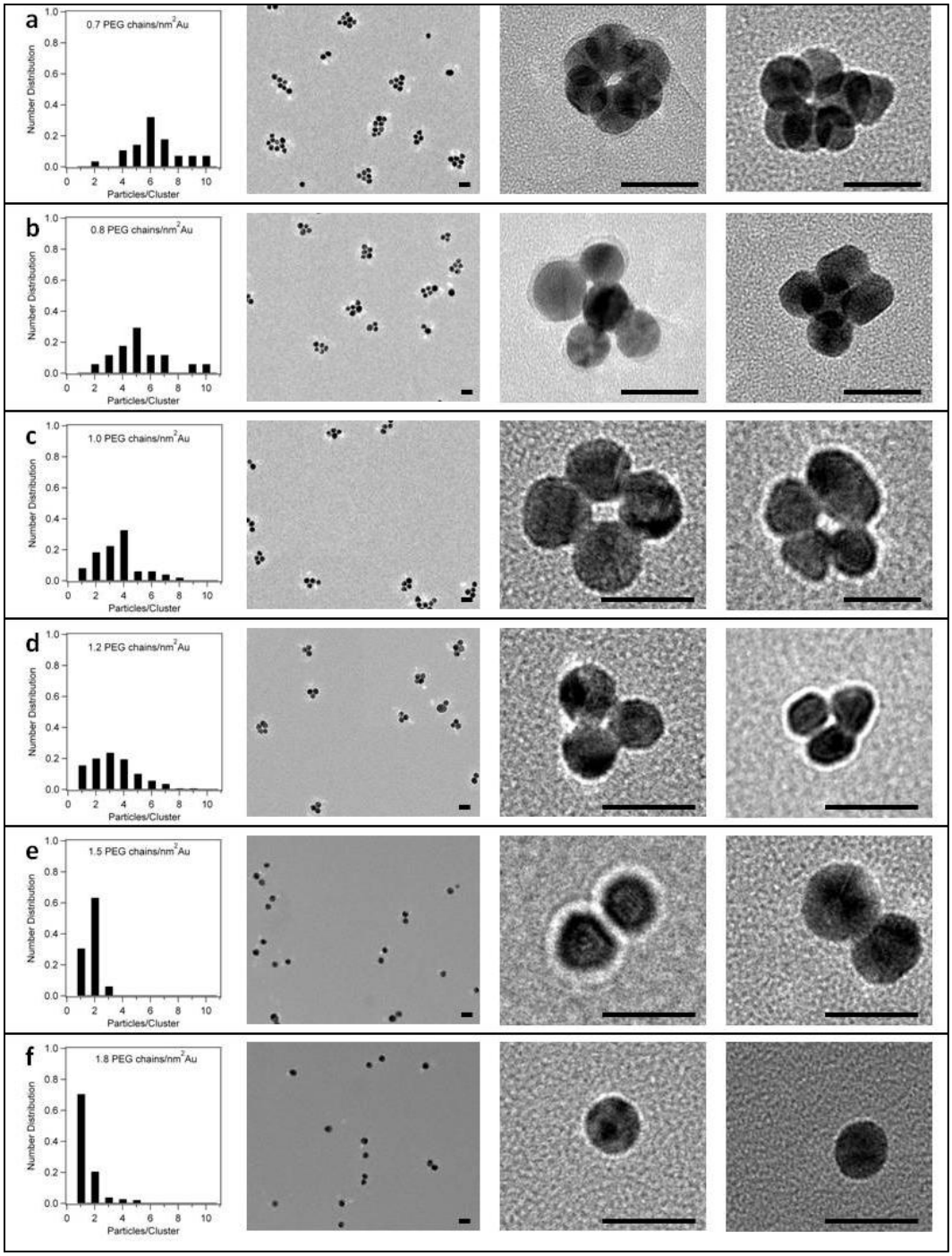

Figure S12. Histograms of the number of particles per cluster for (a) 0.7 PEG chains/nm^2 Au, (b) 0.8 PEG chains/nm^2 Au, (c) 1.0 PEG chains/nm^2 Au, (d) 1.2 PEG chains/nm^2 Au, (e) 1.5 PEG chains/nm^2 Au and (f) 1.8 PEG chains/nm^2 Au. Examples of clusters observed for each sample are to the right (scale bar = 20nm).

Cluster Stability

The clusters presented in this work are stable for several months. Figure S13 show excellent agreement between 0.7 PEG chains/nm^2 Au octane-thiol functionalized clusters after 1 week and after 5 months of aging. No sedimentation occurred during this time either.

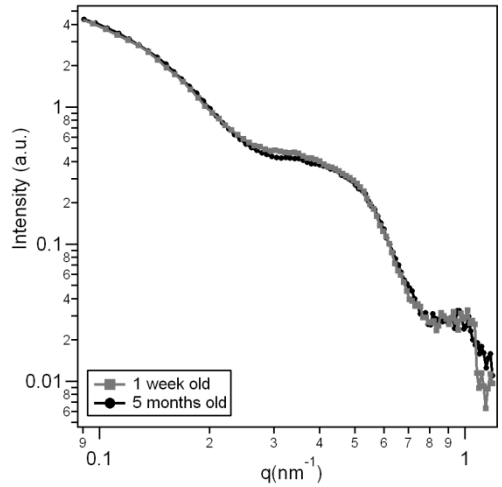

Figure S13. SAXS experimental curves for an octane functionalized 0.7 PEG chains/nm^2 Au clusters after 1week and 5 months.

In Figure S14, SAXS experiments show that particle clusters in our system are stable over a broad range of temperatures (5-50ºC). No change in the shape of the clusters is observed throughout this temperature range and all the scattering curves overlap perfectly on top of each other. In other cluster systems, stabilized by balanced electrostatic interactions, a strong temperature dependence is usually observed.[5]

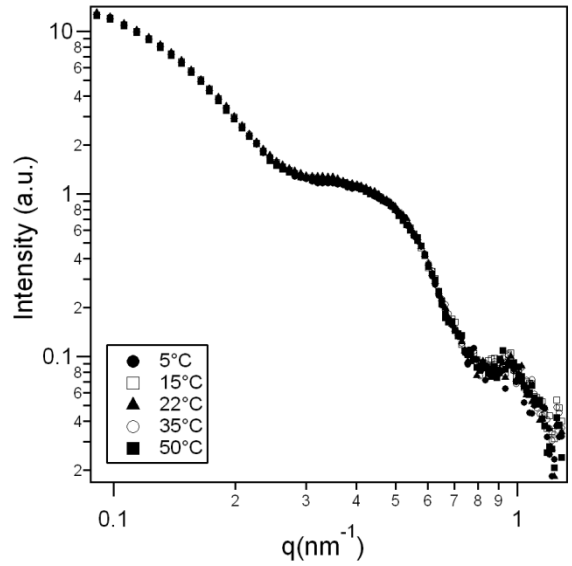

Figure S14. SAXS experimental curves for an octane functionalized 0.7 PEG chains/nm^2 Au cluster at varying temperature.

The primary gold particles in our system are originally stabilized by negative surface charges from citrate adsorption.[6] The zeta potential of the dispersions was quantified using phase analysis light scattering (PALS) as a function of the surface modification. As expected, the original gold particles show the largest zeta-potential (negative) due to the surface charge of the citrate cap that stabilizes them during synthesis. There is a decrease in the magnitude of the zeta potential after functionalizing with PEG that is explained by shifting the shear plane away from the particle surface. The zeta potential is also reduced further after functionalizing with octane-thiol because the adsorbed citrate is displaced by the alkane thiol.

SAXS data in Figure S15, shows that the ionic strength does not have any effect on the final cluster structure. The octane-functionalized 1.0 PEG chains/nm^2 Au clusters with 0, 25 and 50 mM NaCl showed no difference and are exactly on top of each other.

Table S2.

	No Alkane	Octane
Bare Gold	-81.8 mV	
0.3 PEG chains/nm^{2}Au	-68.7 mV	-53.1 mV
2.4 PEG chains/nm^{2}Au	-61.9 mV	-47.8 mV

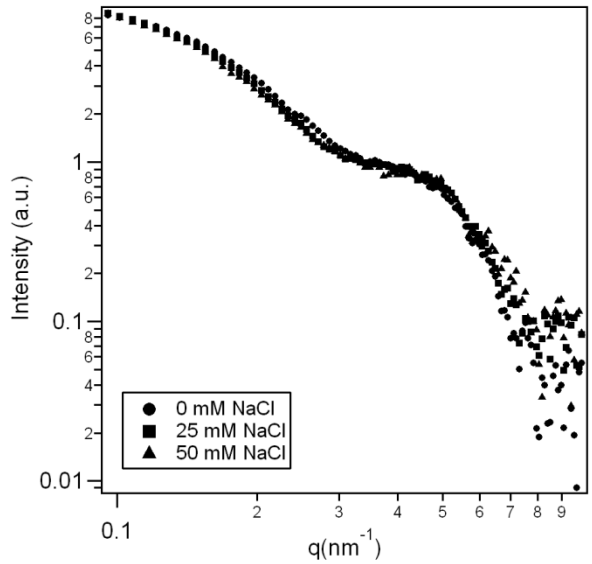

Figure S15. SAXS experimental curves for octane functionalized 1.0 PEG chains/nm^2 Au clusters at 0mM, 25mM and 50mM NaCl.

References

1. J. Shan and H. Tenhu, *Chemical Communications*, 2007, 4580-4598.
2. P. Debye, *Annalen Der Physik*, 1915, **46**, 809-823.

3. Rayleigh, *Proceedings of the Royal Society of London Series a-Containing Papers of a Mathematical and Physical Character*, 1911, **85**, 471-473.
4. P. Linder and T. Zemb, eds., *Neutrons, x-rays and Light: Scattering Methods Applied to Soft Condensed Matter*, Elsevier Science B. V., Amsterdam, 2002.
5. A. Stradner, H. Sedgwick, F. Cardinaux, W. C. K. Poon, S. U. Egelhaaf and P. Schurtenberger, *Nature*, 2004, **432**, 492-495.
6. G. Frens, *Nature-Physical Science*, 1973, **241**, 20-22.